

Vulnerabilities of Electric Vehicle Battery Packs to Cyberattacks on Auxiliary Components

Shashank Sripad^a, Sekar Kulandaivel^b, Vikram Pande^a, Vyas Sekar^{b,1}, and Venkatasubramanian Viswanathan^{a,1}

^aDepartment of Mechanical Engineering, Carnegie Mellon University, Pittsburgh PA 15213; ^bDepartment of Electrical and Computer Engineering, Carnegie Mellon University, Pittsburgh PA 15213

This manuscript was compiled on October 28, 2022

Modern automobiles are entirely controlled by electronic circuits and programs which undoubtedly exposes them to the threat of cyberattacks. Alongside, there is a potential for massive growth in electric vehicle (EV) adoption. The cyber vulnerabilities are magnified with electric vehicles because of the unique and critical risks that entail most EV batteries. EV battery packs provide ‘limited driving range’ and have ‘finite lifetime’, and there is widespread anxiety regarding range and life. In this study, we develop a systematic framework to model cyberattacks on auxiliary components and identify the consequent impact on EV batteries. We model the possible cyberattacks on auxiliary components by engaging them in various ‘modes’ and analyze the impact on battery packs described through a physics-driven experimentally-validated model that accurately captures battery dynamics and degradation. In the short-term, cyberattacks could deplete a battery pack by up to 20% per hour and completely drain the available range. The EV battery pack is most vulnerable to cyberattacks when it is fully charged due to the influence of state-of-charge (SOC) on the battery health. For long-term impact, we explore the location effect of attack and identify that cyberattacks could cause a 3-fold increase in the internal resistance (an indicator of cycle life) in cold regions versus hot regions. We believe that the methodology and the approach presented will help in building the foundational principles for cyber-security in the context of electric vehicles; a very nascent but crucially important topic in the coming years.

electric vehicles | automotive cyber-security | Li-ion batteries | battery degradation

The modern automobile has all of its ‘workflows’ controlled by electronic circuits, and the provision of additional features and wireless instruments renders the vehicle vulnerable to a host of cyberattacks. The area of automotive cyber-security has received significant attention over the past few years (1, 2) and demonstrated cases of automotive cyberattacks till date have been primarily focused on the possibility of compromising the functionality and safety of automobiles.(1, 2)

Alongside, another notable development in the automotive sector is the transition towards EVs as a response to tailpipe emissions and global warming.(3, 4) The current global stock of over 2 million EVs and HEVs is evidence for the tremendous progress in EV adoption.(5) However, their adoption is still limited by concerns of limited driving range, lifetime, and safety owing to the limitations and potential risks associated with current Li-ion batteries.(6–8)

Given these two emerging trends, a natural question that emerges is the possibility of cyberattacks in undermining the range, life and safety of EV batteries. The hacking

of battery firmware, limited to portable electronics, where the supplanting of routine commands with malicious ones within battery monitoring systems is shown.(9) It is worth highlighting that EV batteries are vastly different from portable electronics in terms of the scale of the systems, conditions of operation, as well as the constituent materials and thus, there exists an enormous gap in understanding the landscape of automotive cybersecurity unique to electric vehicles.

The primary challenges involved in assessing the security concerns of systems involving batteries is due the complex molecular-scale processes occurring inside a closed system. A practical battery system stores a limited amount of energy via reversible electrochemical reactions at each electrode. During normal operation, several unwanted side reactions also occur which eventually degrade the battery’s ability to store energy and thus, reduce the lifetime(10). In addition, any battery system also has a specified set of conditions for safe operation, outside which there is a potential risk of fire due to the flammable electrolytes used in modern batteries (7, 11), an event generally referred to as ‘thermal runaway’ (7). cyberattacks could compromise the driving range of EVs by targeting the stored energy, the lifetime by enhancing the side reactions, and safety by pushing the operating conditions to unsafe limits.

In this article, we develop a physics-driven approach to systematically analyze cyberattacks on EV batteries. Using this approach, we analyze the potential impact of a cyberattack on the driving range of the EV, and secondly, the impact

Significance Statement

Modern automobiles are exposed to a host of cyberattacks and the potential risks that entail such attacks has gained significant attention lately. Alongside, globally, the automotive industry is transitioning towards electric alternatives as a response to the harmful effects of tailpipe emissions. The heart of an electric vehicle, the battery pack, could be the target of such cyberattacks, and the associated risks are both critical and unique. In order to understand and quantify these risks, we need a new paradigm which couples existing automotive cyber-security narratives with the knowledge-base on battery systems, and this study presents the first such model for analysis.

V.S and V.V designed the research, S.S. performed all the battery pack simulations. S.K. and S.S. developed the detectability index. S.S., S.K., V.P., V.S. and V.V. analyzed the results and wrote the paper.

The authors declare no conflict of interest.

¹To whom correspondence should be addressed. E-mail: venkvis@cmu.edu, vsekar@andrew.cmu.edu

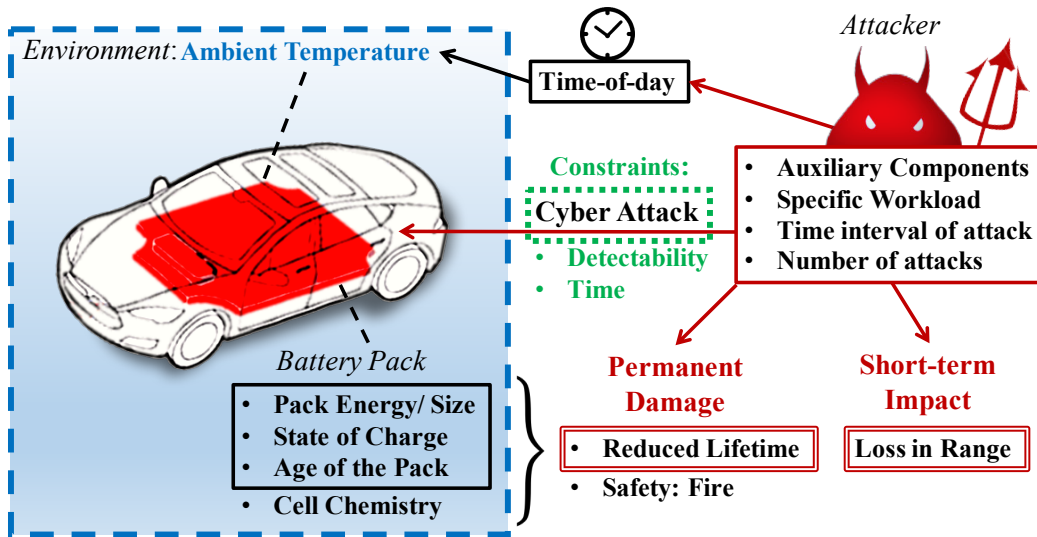


Fig. 1. Pictorial illustration of an attack scenario. The illustration enumerates all the variables that need to be considered for analyzing the impact of a cyberattack. The four sets of variables together define the environment, specify and define the state of the battery pack, provide a description of the variables under the attacker's control, and stipulate the constraints that the attack is subjected to. The attacker employs the control variables with the intention of causing short-term impact in terms of reduction in the range of the vehicle or to cause long-term permanent damage to the battery pack.

on the lifetime of the battery pack. The attack scenarios considered are shown in (Fig. 1), where the attacker is able to gain control of the auxiliary components of the automobile to orchestrate a cyberattack. The different variables that need to be considered for modeling such an attack scenario could be categorized as (i) Environment state variables, (ii) Battery pack state variables, (iii) Attacker's control dimensions, and (iv) Attacker's constraints. Throughout this study, we only consider 'primary' attacks which can compromise systems within the vehicle. It is worth pointing out that 'secondary' attacks which attempt to compromise the infrastructure around EVs like charging stations could also be important. Furthermore, we do not explicitly address the issue of the possibility of fire (7), since a physics-driven understanding of this phenomenon is limited at this stage.

In order to enable this analysis, we systematically compiled the energy consumption pattern of every auxiliary component along with its characteristic power profile. The relevant data for such power profiles is curated from a large number of studies (12–16) where several components in different modes of operation have been analyzed. We believe this dataset will form an important piece for future automotive cybersecurity studies.

The workload of a cyberattack is determined by the instantaneous power consumed and the duration of the attack. In the context of auxiliary components, the cyberattack can engage one or more components in different operating modes for varying periods of time, which forms the control dimensions of the attacker. The workloads cause a quantifiable impact on the functionality of the battery pack and thereby of the vehicle itself. It is worth pointing out that cyberattacks engaging certain components can be easily identified (for e.g. windshield wipers). Further, long term engagement also leads to possible identification (for e.g. air conditioning). Thus, there exists additional constraints on duration of attacks and the choice of components for engaging the attack. We explicitly address this issue by developing a preliminary metric for detectability by systematic categorization of the components.

Results and Discussion

We begin by examining the short-term and long-term impacts of cyberattacks on EV battery packs followed by a discussion on a possible approach to understand the attacker's constraints.

Short-term Impact. Once the auxiliary components are compromised, the attack workloads cause a depletion of energy contained in the battery pack, thereby a reduction in available driving range. Such an impact would play into the well-known issue of 'range anxiety' (17, 18).

For the examination of short-term impact or range reduction, we examine different electric vehicles chosen on the basis of the availability and market share in the United States (19), namely, Leaf manufactured by *Nissan Motor Company Ltd.*, i3 by *BMW AG*, Model S P100D by *Tesla, Inc.*, and e6 by *BYD Auto Co., Ltd.*. The relevant data on the energy consumption, range, and battery pack characteristics for each of these vehicles can be found in the (SI-Text). For all our battery pack analysis, we use a multiphysics thermally coupled Li-ion battery model (20) based on the AutoLion-ST platform. The details and working of the model can be found in the (Methods Section). We have successfully utilized this platform for realistic pack design in a variety of electric vehicle use-cases. (21–23)

The short-term impact of different attack workloads on each of the aforementioned EVs is shown in (Fig. 2). The workload could comprise of either a single component or multiple components engaged at the same time. The important variable in the context of short-term impact is energy consumption, which determines the range of the vehicle. In terms of battery pack state variables, the pack energy or size determines the range based on the energy consumption per unit distance or electric-mileage of the vehicle. In (Fig. 2), we observe the short-term impact by engaging various components is roughly linear in time with the slope being given by the power consumed by the component(s). As would be expected, the high power components such as air conditioning (A/C, 2.6 kW) and Wipers (1.2 kW) lead to the greatest reduction in range. We observe that EVs with smaller battery pack like the Nissan Leaf (30 kWh) or the BMW i3 (33 kWh) are

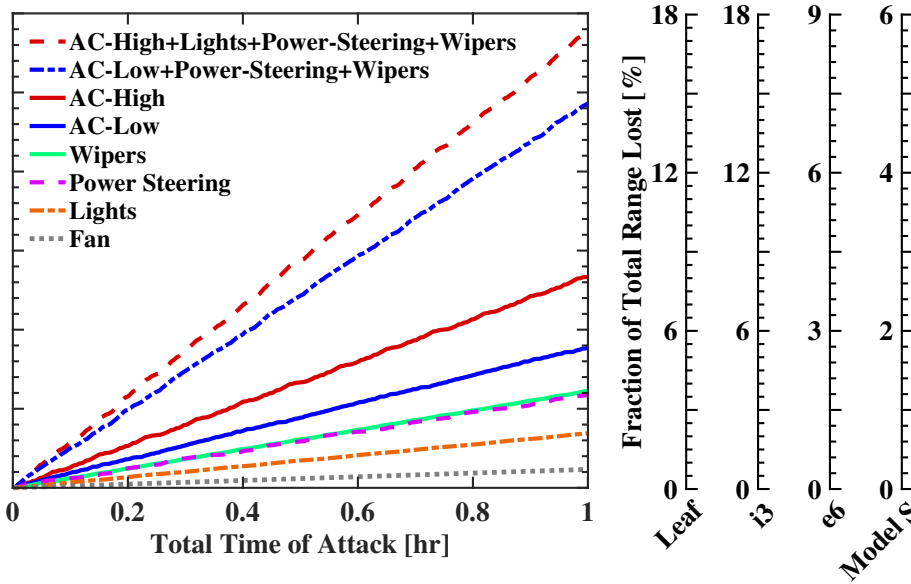


Fig. 2. The fraction of rated range lost due to the cyberattack is determined using the energy consumption per unit distance of the electric vehicle. The energy consumption changes with temperature, where extreme (low of high) temperatures lead to an increased energy consumption. The quantity of range reduced is calculated using the same energy consumption as the one used to calculate the rated range, and hence the fraction of rated range lost is independent of the ambient temperature. Further details of the relevant calculations can be found in the (SI-Text).

impacted to a much greater extent with a loss in range of approximately 20% of the total rated range compared to under 10% for EVs like the Tesla Model S (100 kWh) and the BYD e6 (75 kWh) for an hour-long attack. An important implication of (Fig. 2) is that regions and countries where EV adoption is being proposed with the deployment of EVs with small battery packs for urban commute would face a greater threat from cyberattacks.

It is worth noting that the fraction of total range shown in (Fig. 2) is calculated in the best-case scenario of a fully charged battery pack (100% SOC). However, it is well-known that the average SOC will be well below 100%(24) and approximately half the Tesla EV users maintain a charge-level of 80% or lower(24). Based on this average state of charge, the fractional range reduction could be 25% higher.

The short-term range reduction analysis also highlights the risk to hybrid electric vehicles (HEVs) since most HEVs have much smaller battery packs compared to EVs, and consequently would lose most of the electric driving range in a short span of time. As the battery packs age, the capacity and driving range reduces, and consequently the impact of short-term cyberattacks would be greater. The rate of aging for current EV battery packs is typically low and thus, the age of the pack has minimal effect in the context of short-term impact.

To summarize, short-term impact or range reduction due to a given cyberattack workload is more effective on smaller battery packs at a lower state-of-charge. The impact would also be marginally higher for older battery packs. The move towards smaller battery packs for urban commute faces a huge threat from cyberattacks. In addition, in the urban scenario, the typical state-of-charge of EVs is well below full charge and with limited charging infrastructure available per EV, this represents a serious vulnerability.

Long-term Impact. Assessing long-term impact is challenging due to the prohibitive (and often impractical) ‘time-cost’

associated with actual battery testing.(25) Thus, the only realistic approach to tackling this challenge is to build high-fidelity experimentally validated models coupled with high-precision testing for a short period of time.(26, 27)

The primary mechanism responsible for cell degradation is the growth of the solid-electrolyte interphase (SEI) layer at the graphite anode of a Li-ion battery.(28) The layer grows as a result of solvent reduction at the anode-electrolyte interface which consumes Li^+ ions, thereby causing a decrease in the amount of active Li^+ ions available and loss in capacity. A model for the current density of the rate of SEI formation is given by:

$$j_{\text{SEI}} = -k_{\text{SEI}}c_{\text{sol}} \exp\left(\frac{\alpha F}{RT}(\phi_1 - \phi_2 - \frac{\delta}{\kappa_{\text{SEI}}}(j_{\text{in}} + j_{\text{SEI}}))\right), \quad [1]$$

The details of each of the variables can be found in (SI-text). In addition to loss in capacity, the thickness of the SEI layer increases the internal resistance or impedance of the cell, thereby leading to a loss in the power capabilities.

We propose that the long-term impact of a cyberattack can be quantified using the increase in thickness of the SEI layer or equivalently by the increase in internal resistance due to the attack. The EV battery pack end-of-life is characterized by degradation in capacity to 80% of the initial capacity (29). The usable 20% of the capacity can be called the ‘vital capacity’ of the battery pack, and the variations in each of the state variables like temperature, state-of-charge, pack size, pack age, etc. affect the degradation in vital capacity in a different manner. A parametric analysis of all the variables was carried out, shown in (SI-figures), to explore the effect of each variable on the damage to vital capacity and thereby identify the variables which influence the degradation process to the greatest extent.

The damage to vital capacity as a function of ambient temperature during the cyberattack displays the well-known Arrhenius relationship (30) as seen in (SI-figure). Attacking a battery

pack at higher operating temperatures, or in other words, a time-of-day when the temperature is higher or in geographical locations where the ambient temperature is higher would lead to a greater damage to vital capacity. Evaluating the effect of temperature along with variations in the state-of-charge of the battery pack can be seen in (SI-figure), based on which we can conclude that cyber-attacks conducted on fully charged battery packs would have a much greater impact than attacks on depleted packs. The time-window after an EV battery pack is fully charged is when the battery is at its highest state-of-charge, and hence is the point when the EV is most vulnerable.

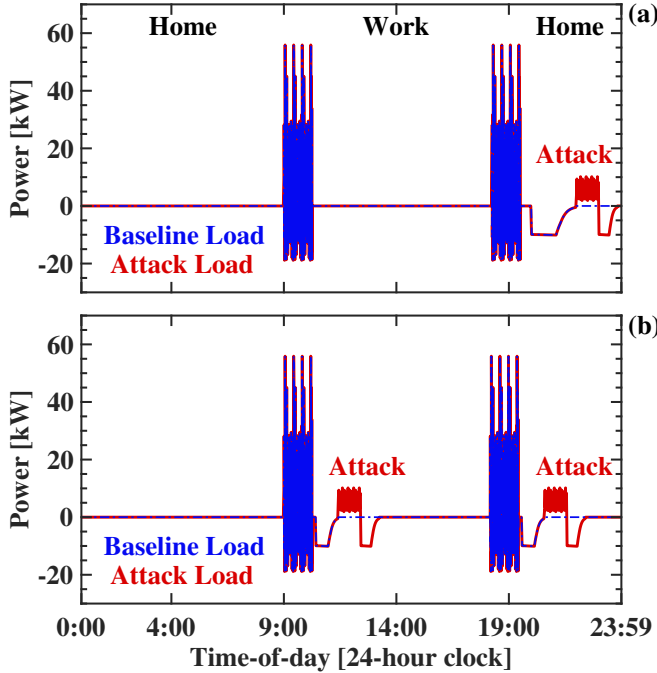


Fig. 3. The daily power load on the Model S P100D which shows multiple scenarios. The power load shown in 'blue' represents the baseline scenario where we have no cyberattacks, and the 'red' represents the attack scenario. The attack is assumed to take place only during the time-window after charging based on the conclusions drawn from the our analyses above. The case where the user charges only at home is illustrated in (a) while (b) is a case where the user charges both at home and at work. The attack scenario in the work-charging case could have two distinct sub-cases where the attack is conducted either at one or both the time-windows after charging.

An important question emerges on whether age of the pack plays a role in determining the impact of cyberattack. (SI-figure) shows a bi-variate analysis between SOC and temperature for battery packs of different age, where we observe that older packs show a lower magnitude damage for the same attack workload. Further, we observe a monotonic decrease in the magnitude of damage with every successive attack for the same attack workload. (SI-Figure) shows this quantitatively, illustrating the damage to vital capacity as a function of the time taken by different attack workloads. This shows that damage to vital capacity is a sub-linear function of the total time of attack and age of the pack, characteristic of a diffusion-limited process.

The effect of the nature of the power profile of a workload can be studied using the metrics of cumulative energy consumption, the average power, and the rate of change in

power. In (SI-Figure), we observe that while the damage to vital capacity increases linearly with increase in the cumulative energy consumption and average power, the effect of an increase in the differential of power is minimal. Alternatively, what we see is that the magnitude of the discharge rates induced due to auxiliary components is not large enough to have a significant effect on the damage to vital capacity, consistent with prior experimental predictions of the capacity fade with rate of discharge (30).

Using an attack workload that is more energy intensive or attacking a battery pack that is smaller have an equivalent effect, since the metric needed to assess is the depth-of-discharge (ΔDOD) due to the workload. We observe a linear relationship between the ΔDOD and the damage to vital capacity (SI-Figure). It follows that workloads which employ energy intensive components or workloads with multiple components engaged together, would cause a greater impact on the battery pack. Although, the increase in the magnitude of damage due to workloads with higher energy consumption is not significant, as seen in (SI-Figure) from the small slope of the linear relationship. A 'row-hammer' attack scenario based on the same concept is that of exerting the attack workload on a few rows of cells within the pack. Under such a scenario the ΔDOD increases linearly with the decrease in number of rows. As shown in (SI-figure), such an attack would magnify the damage on the rows of the cells under attack and would accelerate the degradation to end-of-life.

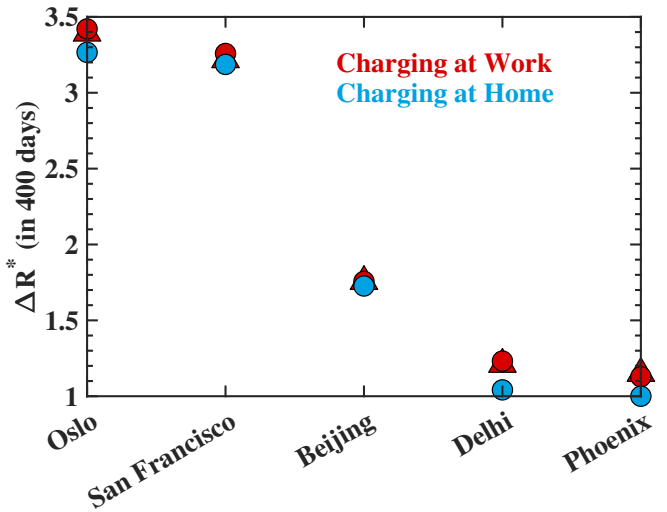


Fig. 4. We can study the long-term impact of cyberattacks here based on the results of simulating the power loads shown in (Fig. 3) for ~ 400 days. ΔR^* represents the relative increase in the resistance of the cell due to the cyberattack when compared to the baseline scenario. Each geographical location shown is incorporated using the variations in ambient temperature over the year. The triangular markers indicate situations where both time-charging after charging in the work-charging case are exploited to attack and in such cases the average ΔR^* of the two attacks is shown in the figure, while the circular markers represent the cases where only one cyberattack. The data used to incorporate the ambient temperature variations can be seen in (SI-figure)

Based on the parametric study summarized above, we can now describe critical attack workloads that are possible and examine them in real-world scenarios. The combination of components chosen for an attack aimed to cause greater

impact would be a combination shown in (Fig. 2) which uses high-powered air-conditioning, along with lights, wipers, and the power-steering. The results from the parametric analysis of the state-of-charge suggests that the attack should be conducted after the pack is charged completely, and hence we need to design the attack scenario accordingly. We consider two types of EV users as shown in (Fig. 3), the first is a user who only charges the battery pack at ‘Home’ and the other is a user who charges at ‘Home’ and at ‘Work’. In the former case we have only instance to attack, while the latter case has two instances for the attack. We analyze the cases where these users are located in Oslo, San Francisco, Beijing, Delhi and Phoenix. These locations are chosen to represent a range of temperatures and including potential locations where there could be substantial EV penetration. We also limit the total time for attack to one hour due to the constraints of detectability, which will be discussed later. Another aspect to note here is the apparent analogy between our current approach to assessing long-term damage from cyberattacks and discussions on damage to EV batteries from the Vehicle-to-Grid (V2G) model(31), but an important distinction between the two situations is that the in the latter, the user controls whether or not the EV participates in the V2G model, whereas, in the context of cyberattacks the user has no control. It follows that, the findings from our analysis would have implications on the approaches to assess damage for V2G scenarios as well.

In order to assess the permanent damage caused due to the cyberattack in real-world scenarios shown in (Fig. 3), we propose the use of a normalized quantity, ΔR , which represents in the increase in internal resistance of the cell as compared to a cell within a pack which has not been subjected to the attack workloads. ΔR provides information on the effectiveness of the cyberattack. We calculate ΔR after 400 days for each case using the following relationship,

$$\Delta R = \frac{R_{SEI}^A - R_{SEI}^B}{R_{SEI}^B}, \quad [2]$$

where R_{SEI} is the resistance due to the SEI layer, and ‘A’ and ‘B’ represent the attack and baseline scenario. For the quantities reported in (Fig. 4), ΔR^* values are obtained by normalizing all the ΔR values with the minimum value in a given set.

In (Fig. 4), we observe an interesting result regarding location that the relative increase in internal resistance is the most for Oslo, which has the lowest average ambient temperature. This appears to be in contradiction with earlier analysis that shows that higher temperature leads to greater damage to vital capacity. While an increase in ambient temperature causes an increase in the thickness of the SEI layer, the resistance due to the formation of SEI layer impedes further growth. This phenomenon leads to the fact that places like Phoenix, where the ambient temperature is high, already feature a substantial SEI layer thickness, thereby minimizing any additional damage to vital capacity due to the attack workload. It is worth highlighting however, that the average resistance due to the SEI film formed is higher in warmer regions compared to colder regions.(32) Comparing the two scenarios of an attack after charging at home versus at work, there is minimal effect on

the damage to vital capacity, since the average temperature between the two cases is nearly the same. This analysis suggests that the extent of damage is highest for colder regions, but largely independent of attack timing. In (Fig. 4) we can also study the second case which is that of two attack sequences, one at Work and the other at Home, which is possible in the Work charging scenario.

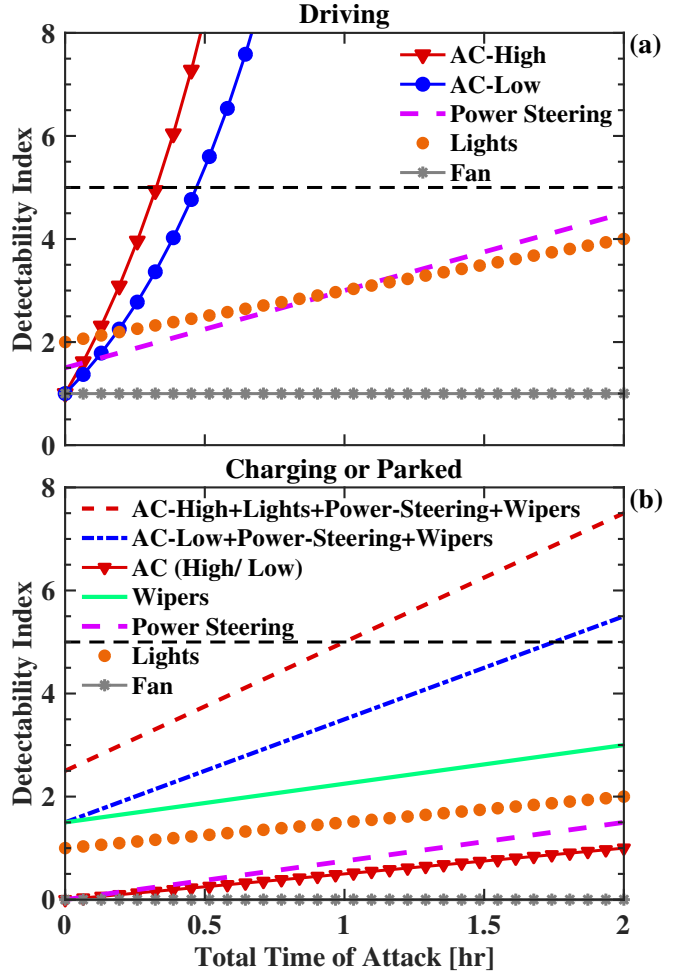


Fig. 5. Detectability Index for the various auxiliary components considered for two cases (a) When the user the driving (b) When the EV is charging or at rest in a parked state, where the detectability index limit is assumed to be 5. Components like Air-Conditioners have an exponential rise in the detectability index in the driving case while in the resting or charging scenario we observe a much lower detectability for the same. When more than one component is engaged the detectability limit is exceeded in the driving scenario and hence do not feature in the first case.

Attack Constraints. An important limitation on the attack is the ability to be detected and the detection process is a highly probabilistic quantity that depends on many different factors. Here, we propose a simplistic model towards handling this complex issue. We develop a quantity, which we term ‘detectability index’ for each component which is a function of time, that measures the degree to which an attack on that component can be detected. The methodology for calculating the detectability index is based on the evaluation of three primary detectable indices associated with a given auxiliary component, (i) physical actuation, (ii)

notification regarding the engagement of component and (iii) the component's effects on the environment. For example, a component like an air-conditioner would involve physical actuation which can be detected due to the audibility of the fans and compressors, with user notifications which indicate the component has been engaged, and finally cause a change in temperature and humidity over time. The detectability index, is examined in two scenarios, when the user is driving or when the EV is at rest. A more detailed discussion on the methodology followed in the development of detectability index can be found in (SI-text) and (SI-figures).

The detectability index limit is chosen to be five at which point, it is very likely that the attack will be detected. The detectability index of an attack workload with more than one component engaged at the same time would be a linear combination of the detectability indices of each of the engaged components. Among the easily detectable quantities while driving, our index identifies that A/C can be detected in about 20 minutes. However, such an attack while charging or when parked could go undetected for several hours. Engaging multiple components (for e.g. power steering and lights) while driving leads to quite easy detectability within an hour. All of these factors highlight that the maximum likelihood of a cyberattack going undetected is when the vehicle is parked or charging. It is worth highlighting that average vehicle is idle and unused for well-over 90% of the time.(33)

Conclusions. We have analyzed the potential impact of cyberattacks utilizing the auxiliary components alone without compromising the battery managements systems or the infrastructure setup around EVs like charging. Auxiliary components are seen to cause significant short-term by depleting the available range and potential long-term impact on battery packs by enhancing the side reactions that damage the battery. Attacks lasting just a few hours that engage a combination of energy intensive components could completely deplete the battery pack and as discussed previously this could have serious implications on EV adoption proposals. With our analysis of long-term damage highlights the importance of developing a phenomenological models of the degradation process. Using metrics like ΔR would have implications for analyses of damage in other contexts as well, like damage to EV batteries in V2G scenarios.

While the effect of engaging auxiliary components has the potential to cause limited damage, we believe the damage possible during charging could be much more substantial. Cyber vulnerabilities related to charging is much less developed and this will form the focus of our future investigations. In the context of EVs we have emphasized on the critical nature of the battery pack and we need a more systematic mapping of the automotive (EV) networks to incorporate the several aspects discussed above including the compromise and abuse of auxiliary components. In addition, these approaches could also be incorporated in battery management systems of the future, where accurate and precise control systems could be used both to monitor metrics like ΔR along new mechanisms to detect the compromise of EV networks.

Materials and Methods

The 1D+1D or Pseudo 2D model used to simulate the battery pack operation is discussed here. Other details on the power load of the auxiliary components and the energy consumption of EVs can be found in the (SI-Text).

Battery Modeling. These equations used for the battery modeling are summarized by Fang et al.,(34) and Kalupson et al., (20) using Eqns. (3-7) which describe the 1-D transport model for the species and the charge coupled with a lumped thermal model. The solid phase charge conservation is given by

$$\nabla \cdot (\sigma^{\text{eff}} \nabla \Phi_s) = j^{\text{Li}}, \quad [3]$$

where σ^{eff} is the effective electronic conductivity and Φ_s is the potential of the solid phase. The electrolyte phase charge conservation is given by

$$\nabla \cdot (k^{\text{eff}} \nabla \Phi_e) + \nabla \cdot (k_D^{\text{eff}} \nabla \log(c_e)) = -j^{\text{Li}}, \quad [4]$$

where k^{eff} is the effective ionic conductivity, Φ_e is the potential of the electrolyte phase, k_D^{eff} is the conductivity and c_e is volume averaged Li concentration in the electrolyte phase. The conservation of species in the electrolyte phase is given by

$$\frac{\partial(\varepsilon_e c_e)}{\partial t} = \nabla \cdot (D_e^{\text{eff}} \nabla c_e) + \frac{(1 - t_+^0)}{F} j^{\text{Li}}, \quad [5]$$

where ε_e is the volume fraction, D_e^{eff} is the effective diffusion coefficient, t_+^0 is the transference number, and F is the Faraday constant. The species conservation in solid phase is given by

$$\frac{\partial c_s}{\partial t} = \frac{D_s}{r^2} \frac{\partial}{\partial r} (r^2 \frac{\partial c_s}{\partial r}), \quad [6]$$

where c_s is the concentration of Li in the solid phase, D_s is the diffusion coefficient in the solid phase, and 'r' represents the radius of the particles of active material. The energy balance is represented as a lumped thermal model given by

$$\frac{\partial(\rho C_p T)}{\partial t} = (q_r + q_j + q_c + q_e) A_{\text{cell}} + h_{\text{conv}} A_s (k \nabla T), \quad [7]$$

which accounts for q_r reaction heat, q_j the joule heating, q_c the heating due to contact resistance between the current collector and electrode materials, and q_e the entropic heating. The last term represents the heat dissipation, where h_{conv} is the coefficient of heat dissipation and A_s is the cell external surface area.

Degradation Process. An SEI film growth model is used to quantify the loss of active Li-ions and is modeled in a manner similar to other well-known studies(28).

$$\frac{d\delta_{\text{SEI}}}{dt} = -\frac{j_{\text{SEI}} M_{\text{SEI}}}{2F \rho_{\text{SEI}}}, \quad [8]$$

where M_{SEI} and ρ_{SEI} are the molecular weight and the density of the SEI. The resistance due to the SEI is calculated using the effective conductivity of the electrolyte (solvent) through the SEI using:

$$R_{\text{SEI}} = \frac{\delta_{\text{SEI}}}{\kappa_{\text{SEI}}^{\text{eff}}}, \quad [9]$$

ACKNOWLEDGMENTS. S. S., S. K., V.S. and V. V. gratefully acknowledge support from Technologies for Safe and Efficient Transportation University Transportation Center. V.S. and V. V. gratefully acknowledges support from the Pennsylvania Infrastructure Technology Alliance, a partnership of Carnegie Mellon, Lehigh University and the Commonwealth of Pennsylvania's Department of Community and Economic Development (DCED).

References

1. Koscher K, et al. (2010) Experimental security analysis of a modern automobile in 2010 *IEEE Symposium on Security and Privacy*. (IEEE), pp. 447–462.
2. Checkoway S, et al. (2011) Comprehensive experimental analyses of automotive attack surfaces. in *USENIX Security Symposium*. (San Francisco).
3. Tessum CW, Hill JD, Marshall JD (2014) Life cycle air quality impacts of conventional and alternative light-duty transportation in the united states. *Proceedings of the National Academy of Sciences* 111(52):18490–18495.
4. Laser M, Lynd LR (2014) Comparative efficiency and driving range of light-and heavy-duty vehicles powered with biomass energy stored in liquid fuels or batteries. *Proceedings of the National Academy of Sciences* 111(9):3360–3364.
5. International Energy Agency I (2017) Global EV Outlook, Technical report.
6. Crabtree G, Kócs E, Trahey L (2015) The energy-storage frontier: Lithium-ion batteries and beyond. *MRS Bulletin* 40(12):1067–1078.
7. Abada S, et al. (2016) Safety focused modeling of lithium-ion batteries: A review. *J. Power Sources* 306:178–192.
8. Lisbona D, Snee T (2011) A review of hazards associated with primary lithium and lithium-ion batteries. *Process Safety and Environmental Protection* 89(6):434–442.
9. Miller C (2011) Battery firmware hacking. *Black Hat USA* pp. 3–4.
10. Santhanagopalan S, Guo Q, Ramadass P, White RE (2006) Review of models for predicting the cycling performance of lithium ion batteries. *J. Power Sources* 156(2):620–628.
11. Wang Q, et al. (2012) Thermal runaway caused fire and explosion of lithium ion battery. *J. Power Sources* 208:210–224.
12. Hendricks TJ (2001) Vehicle Transient Air Conditioning Analysis: Model Development & System Optimization Investigations, (National Renewable Energy Lab., Golden, CO.(US)), Technical report.
13. Johnson VH (2002) Fuel used for vehicle air conditioning: a state-by-state thermal comfort-based approach, (SAE Technical Paper), Technical report.
14. Perrucci GP, Fitzek FH, Widmer J (2011) Survey on energy consumption entities on the smart-phone platform in *Vehicular Technology Conference (VTC Spring), 2011 IEEE 73rd*. (IEEE), pp. 1–6.
15. Lawrence CP (2007) Master's thesis (University of Waterloo).
16. Andersson C (2004) Ph.D. thesis (Lund University).
17. Rauh N, Franke T, Krems JF (2015) Understanding the impact of electric vehicle driving experience on range anxiety. *Human factors* 57(1):177–187.
18. Neubauer J, Wood E (2014) The impact of range anxiety and home, workplace, and public charging infrastructure on simulated battery electric vehicle lifetime utility. *J. Power Sources* 257:12–20.
19. Fuels Data Center A (2017) "U.S. Plug-in Electric Vehicle Sales by Model" (<https://www.afdc.energy.gov/data/10567>). Published Data, Accessed Date: 06-September-2017.
20. Kalupson J, Luo G, Shaffer CE (2013) Autolion™: A thermally coupled simulation tool for automotive li-ion batteries, (SAE Technical Paper), Technical report.
21. Sripad S, Viswanathan V (2017) Evaluation of current, future, and beyond li-ion batteries for the electrification of light commercial vehicles: Challenges and opportunities. *J. Electrochem. Soc.* 164(11):E3635–E3646.
22. Sripad S, Viswanathan V (2017) Performance metrics required of next-generation batteries to make a practical electric semi truck. *ACS Energy Lett.* 2(7):1669–1673.
23. LeVine S (2017) Researchers try to crack Tesla's Model 3 Battery (<https://www.axios.com/researchers-try-to-crack-teslas-wall-of-silence-on-its-model-3-battery-2470036723.html>). Online Article, Accessed Date: 22-October-2017.
24. (2017) "Tesla Max Range Battery Survey" (<https://docs.google.com/spreadsheets/d/t024bMoRiDPIDialGnuKPsG/edit#gid=490778289>). Crowd-sourced survey, Accessed Date: 06-September-2017.
25. Ramadesigan V, et al. (2012) Modeling and simulation of lithium-ion batteries from a systems engineering perspective. *J. Electrochem. Soc.* 159(3):R31–R45.
26. Fathi R, et al. (2014) Ultra high-precision studies of degradation mechanisms in aged li-coo2/graphite li-ion cells. *Journal of The Electrochemical Society* 161(10):A1572–A1579.
27. Smith A, Burns JC, Zhao X, Xiong D, Dahn J (2011) A high precision coulometry study of the sei growth in li/graphite cells. *Journal of The Electrochemical Society* 158(5):A447–A452.
28. Safari M, Morcrette M, Teyssot A, Delacourt C (2009) Multimodal physics-based aging model for life prediction of li-ion batteries. *J. Electrochem. Soc.* 156(3):A145–A153.
29. Wood E, Alexander M, Bradley TH (2011) Investigation of battery end-of-life conditions for plug-in hybrid electric vehicles. *J. Power Sources* 196(11):5147–5154.
30. Choi SS, Lim HS (2002) Factors that affect cycle-life and possible degradation mechanisms of a Li-ion cell based on LiCoO₂. *J. Power Sources* 111(1):130–136.
31. Richardson DB (2013) Electric vehicles and the electric grid: A review of modeling approaches, impacts, and renewable energy integration. *Renewable and Sustainable Energy Reviews* 19:247–254.
32. Lawder MT, Northrop PW, Subramanian VR (2014) Model-based sei layer growth and capacity fade analysis for ev and phv batteries and drive cycles. *Journal of The Electrochemical Society* 161(14):A2099–A2108.
33. Wu Q, et al. (2010) Driving pattern analysis for electric vehicle (ev) grid integration study in *Innovative Smart Grid Technologies Conference Europe (ISGT Europe), 2010 IEEE PES*. (IEEE), pp. 1–6.
34. Fang W, Kwon OJ, Wang CY (2010) Electrochemical–thermal modeling of automotive li-ion batteries and experimental validation using a three-electrode cell. *Int. J. Energy Res.* 34(2):107–115.

Supporting Information for Vulnerabilities of Electric Vehicle Battery Packs to Cyberattacks on Auxiliary Components

Shashank Sripad et al.

Supporting Information (SI)

SI Text. Fraction of Range Reduction and the Effect of Temperature: The ambient temperature has a significant impact on the rated range and the use of auxiliary components like heaters and air-conditioners at low or high ambient temperatures causes an additional loss in range. The SOC could have an effect on the discharge efficiency of the battery pack and hence would affect the energy consumption. An aged battery pack would have a lower pack energy, and hence a lower overall rated range. For more details on the impact of each of these variables on short-term impact. The loss in range is determined by the energy consumed by the auxiliary components and the energy consumption of the vehicle at the time instant of the attack. In effect, the fraction of range lost or the ratio of range lost due to a cyber attack and the rated range of the vehicle would be independent of the temperature.

Parametric Analysis: Throughout this study, we examine capacity fade considering a quantity defined as ‘vital capacity’ which is equivalent to 20% of the initial capacity of the battery pack. For EVs a degradation of 20% of the initial capacity or 100% of the vital capacity marks the end-of-life of the battery pack (29). In order to examine in each variables, we select a sample cyber attack defined by a specific workload on the pack conducted for a fixed duration of time. In other words, we fix all the attacker’s control dimensions and constraints. We also fix all other battery pack and environment state variables apart from the variable in consideration, and thereby examine permanent damage as a function of the given variable alone. For examining permanent damage, the first variable considered for analysis is the ambient temperature. The damage to vital capacity is observed to be an exponentially increasing function of ambient temperature and follows the Arrhenius relationship.

The next set of parameters considered are the battery pack state variables. The damage to vital capacity increases linearly with a reduction in the battery pack size. This could be explained as capacity fade being a linear function of the depth-of-discharge since a smaller battery pack would have a larger depth of discharge for the same auxiliary component or workload considered, and this corroborates the findings of other studies (32).

The SOC along with temperature are studied to see their influence on the capacity fade for battery packs of different age, namely 0, 1, and 2-year-old packs as visualized in (Fig. S2). We observe that the damage to vital capacity increases with increase in SOC, in other words, if a cyber attack is conducted on a fully-charged battery pack or a battery pack which is placed in a higher ambient temperature, then the resultant impact would be much greater.

On comparing the SOC-Temperature results for packs of different age, we observe an interesting trend that older packs show a much lower damage to vital capacity with the same specified cyber attack. This can be explained from the fact that the SEI layer modeled shows a growth rate which is a sublinear function of time, and hence the capacity fade or damage to vital capacity decreases for a battery which has already aged for a certain duration.

Detectability Index: The constraints of detectability that need to be examined are shown in (Fig. S5), where we specify a detectability index to each component as a function of time. The methodology for calculating the Detectability Index is based on the evaluation of three primary detectable indices associated with a given auxiliary component, namely, ‘physical actuation’, ‘dashboard notification’, and changes caused in the environment. For example, a component like an AC would entail a degree of physical actuation which can be detected due to the audibility of the fans and compressors, with dashboard notifications which indicate the component has been engaged, and finally cause a change in temperature and humidity over time. The Detectability Index is examined in two scenarios, either when the user is driving or when the EV is at rest. The Detectability Index limit is assumed to be five in each case examined in the (Fig. S5).

SI Figures. The results of the parametric analysis for long-term damage where damage is studied as a function of each variable, the methodology followed to calculate the detectability index is compiled below, and a visualization of the ambient temperature data for the long-term damage simulations can be seen here:

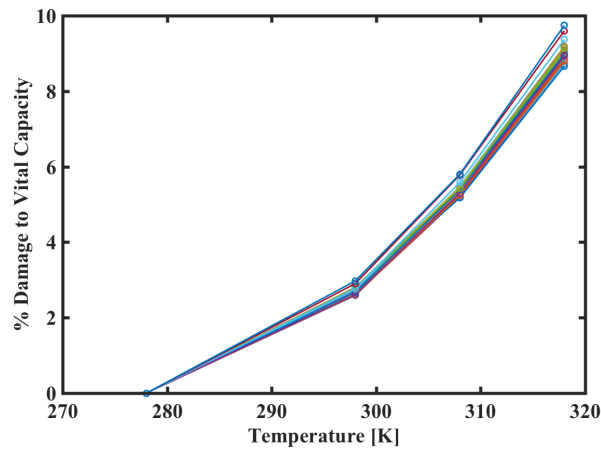


Fig. S1. Damage to Vital Capacity as a function of ambient temperature for various auxiliary components, where we observe the Arrhenius type relationship.

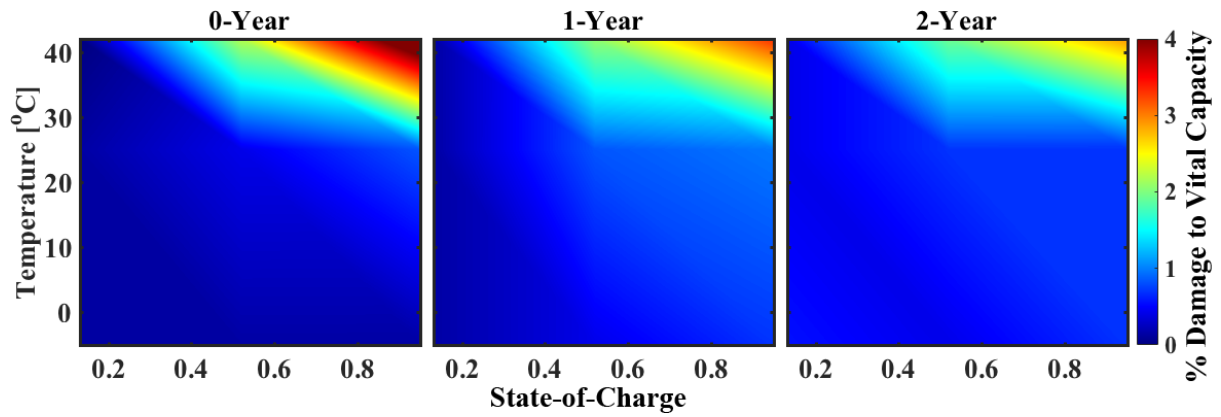


Fig. S2. Bi-variate analysis of the Damage as a function of the SOC and ambient temperature conducted for battery packs of different age (0,1,2 years).

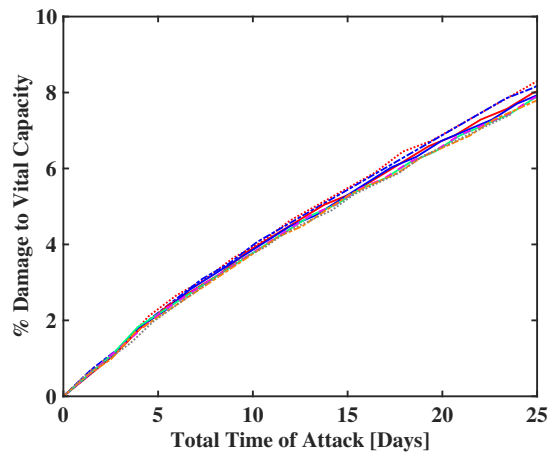


Fig. S3. Damage to vital capacity studied as a function of the total time of attack for various auxiliary components which shows the sub-linear relationship.

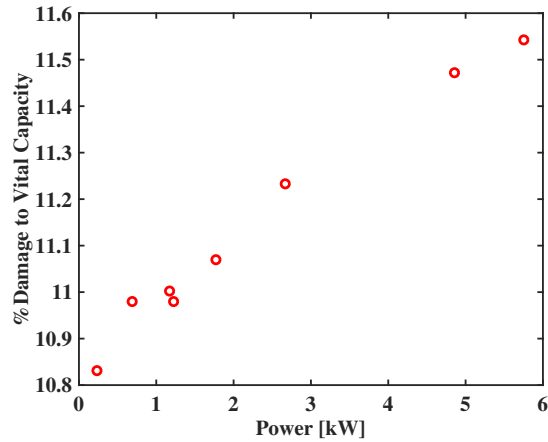


Fig. S4. Damage to vital capacity studied as a function of the energy consumption of the auxiliary components at an ambient temperature of 40°C.

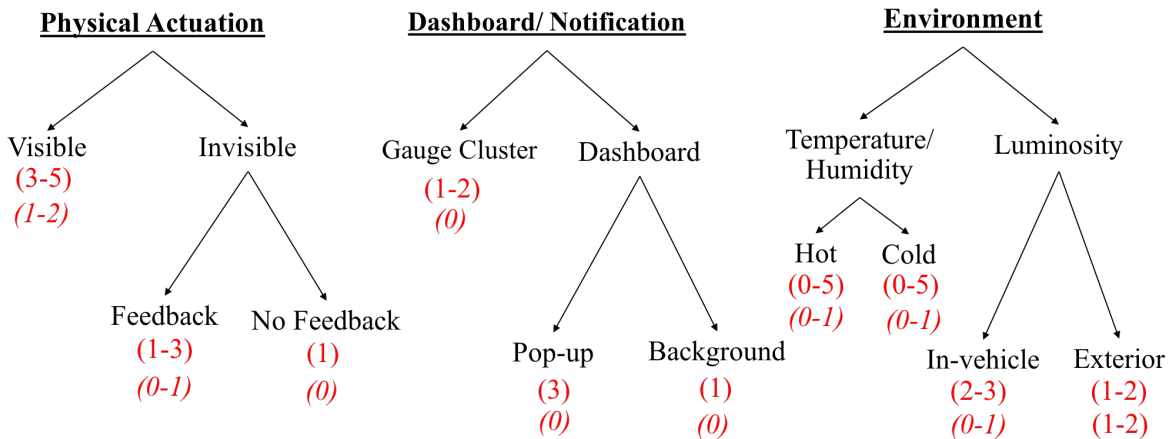


Fig. S5. The basic flowchart for computing the detectability index of various auxiliary components. We see the three categories into which auxiliary components can be classified into, namely, 'Physical Actuation' which includes component like compressors, wipers which involve a moving components. 'Dashboard/ Notification' includes all the components which notify the user about the component being engaged, and lastly the 'Environment' includes components that have an impact on the environment like changes in temperature or humidity. The detectability index values for each of the components is shown with the variable used for categorization where we see two values, the first is the case where the EV is parked and the second where the values are italicized shows the driving scenario.

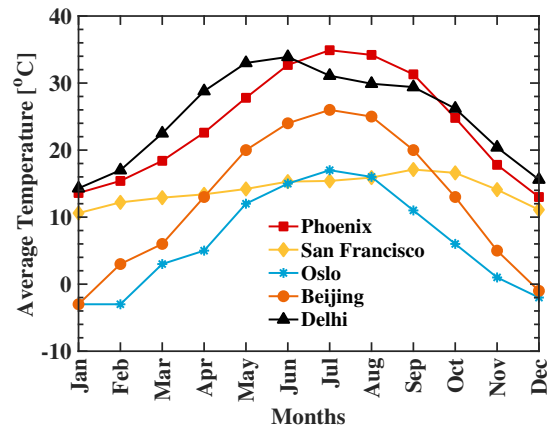


Fig. S6. The temperature variations in different locations over the year used for the long-term damage studies.